AIAA AVIATION Forum
5-9 June 2017, Denver, Colorado
47th AIAA Fluid Dynamics Conference

10.2514/6.2017-3974

Effects of Background Stratification on the Compressible Rayleigh Taylor Instability

Scott A. Wieland*
University of Colorado Boulder, Boulder, CO, 80305, United States

Scott J. Reckinger†
Montana State University, Bozeman, MT, 59717, United States

Peter E. Hamlington‡
University of Colorado Boulder, Boulder, CO, 80305, United States

Daniel Livescu§
Los Alamos National Laboratory, Los Alamos, NM, 87544, United States

Wavelet-based direct numerical simulations of compressible, single-mode Rayleigh-Taylor instability (RTI) have been performed in order to study the effects of background stratification on instability development. Simulations have been performed for different strengths of the initial background stratification, as well as for isothermal, isentropic, and isopycnic conditions. Because interactions of vortical structures play an important role in instability growth, terms in the vorticity transport equation have been analyzed in order to better understand the impact of background stratification on RTI development. The coupling between stratification and vortical structures is further examined using simulations of an analogous case; namely, the evolution of a vortex pair in the presence of background stratification. Background stratifications, regardless of strength or type (e.g., isothermal, isentropic, or isopycnic) generally increase the tendency towards asymmetry between bubble and spike growth, compared to the incompressible case with similar density ratio. This effect is the largest for the isentropic stratification. The simulation with an isothermal background stratification quickly leads to complete suppression of RTI growth at moderate and high stratification strengths. The isentropic case causes an inhibition of the growth and it is unclear under what conditions the growth fully stops. The isopycnic stratification has the least suppressive effect on the instability growth and, at higher strengths, it seems to even have the opposite effect and leads to accelerated growth. These situations can be replicated using arguments based on vortex pair simulations.

I. Introduction

Rayleigh-Tayor instability (RTI) arises when there is a mean density gradient in the direction opposite that of an acceleration. This acceleration can be gravitational or the result of an accelerating front, and the RTI will only appear when there is a perturbed interface in the pathway.[1,2] RTI can be observed in a huge range of systems, from large astrophysical flows to flows at the molecular level, and plays a large part in many engineering systems of interest such as inertial confinement fusion (ICF). A significant portion of these systems, including ICF,[3] supernovae ignition fronts,[4–6] x-ray bursts,[7] and more, involve highly compressible fluid flow effects. Between the acoustic effects, material properties, and various stratifications, it becomes clear that there is not one single parameter that can capture the entirety of compressibility effects on the

*Graduate Research Assistant, Mechanical Engineering, University of Colorado Boulder, Student Member.
†Faculty, Civil Engineering, Montana State University.
‡Assistant Professor, Mechanical Engineering, University of Colorado Boulder, Member.
§Scientist, Computer and Computational Sciences Division, Los Alamos National Laboratory, Associate Fellow.

growth of the instability.[8,9] As the instability continues growing into late times, the characteristics become more nonlinear, chaotic, and unpredictable. It is thus only logical that more of these complex compressible interactions will occur. In short, little is known about these effects on RTI and there is a need to better understand them.[8,10]

Historically, the incompressible case has been the main subject of RTI studies.[11,12] Even in instances where a compressible solver has been used, simulations were carried out in the nearly incompressible regime and, in many cases, additional numerics were added to dampen out what few effects of compressibility are left.[13] In very rare cases, compressibility and background stratification effects have been examined, but none have been robust and complete in their analysis of different stratifications and strengths, leaving knowledge gaps and unanswered questions.[10,14] This has led to the complete picture of compressibility effects on RTI growth not being well understood and thusly, a full investigation using direct numerical simulation (DNS) is needed to uncover any previously unseen physics and to develop better models.

In order to fully resolve all time and length scales associated with compressible RTI, the computational cost is quite high. Between the thin interfaces leading to high gradients, acoustic waves, and even shock waves generated by RTI itself, a very high resolution is needed. In order to reach self-similar or asymptotic states, the simulations require domains that are much longer than the initial perturbation wavelength. Also, the nature of the stratification leads to a range of scales that spans many orders of magnitude in density, pressure, or temperature. In order to satisfy stability requirements, the time step must also be kept quite small. When all of these factors are brought together, it becomes clear that a complex and advanced computational method is needed in order to actually complete the simulations.[15,16]

RTI growth is heavily dominated and influenced by the vorticity dynamics of the problem, through the generation and propagation of vortical structures.[17] For single-mode RTI, the Kelvin-Helmholtz instability on the sides of the moving bubble and spike leads to the generation of vortex pairs in two dimensions and vortex rings in three dimensions. In both cases, the symmetry of the single mode problem results in vortical structures moving both upwards and downwards in the domain. Thus, to better understand the effects of background stratification on the growth of the RTI, simulations of vortex pairs and rings can be carried out in the same stratified medium with no interface present. To be complete, there must be two simulations carried out, one with the induced velocity upwards in the domain and one downwards, in order to capture all of the physics. Analysis of the interactions between the stratified media and the vortical representations can give us insights into the vorticity dynamics of the RTI problem, but at a significantly reduced computational cost.

The rest of this paper discusses the following. First, Section 2 has a discussion of the problem setup and the various background stratifications that will be used in the simulations. Then, in Section 3, there is a brief discussion of the numerical method used to perform these simulations. Section 4 then presents results of RTI simulations for all background stratifications. This is then followed with an analysis of the vorticity dynamics and transport that are responsible for the growth. To complete this discussion, another analysis is performed in which the simplified vortex configurations are investigated and used to further elaborate on the results seen in the RTI problem. Section 5 then finishes the paper with the conclusions.

II. Problem Setup

RTI occurs when a heavier fluid rests on top of a lighter fluid, the interface is perturbed, and there is an accelerative body force such as gravity. As the perturbation begins to grow, the heavy fluid falls into the light fluid to create spike-like structures as the light fluid rises to create bubble-like structures. Initially, if the perturbation amplitude is small, the growth is described by the linearized equations, but as the growth continues, it becomes more and more complex.[1,2] In the early nonlinear stages, vorticity appears at the interface between the two fluids, and potential flow theory can be used to predict a stage of constant velocity growth. Due to the continuing addition of vorticity from the Kelvin-Helmholtz instability on the sides of the bubbles and spikes, the vorticity dynamics quickly become too complex to predict with a simplified model such as potential flow (i.e., the vorticity distribution cannot be understood from simple vortex sheets or point vortices).[8] The interactions lead to a re-acceleration of the bubble/spike growth and late time chaotic development in the classical incompressible case.[17] How these regions are affected by compressibility and stratification is unknown, and the complexity of the problem requires that full DNS be carried out in order to ensure the preservation of all physics in the flow.

Simulations have been performed using the standard multi-species compressible fluid dynamics equations.

The full system of equations is[8,18]

$$\frac{\partial \rho}{\partial t} + \frac{\partial (\rho u_j)}{\partial x_j} = 0, \tag{1}$$

$$\frac{\partial (\rho u_i)}{\partial t} + \frac{\partial (\rho u_i u_j)}{\partial x_j} = -\frac{\partial p}{\partial x_i} - \rho g_i + \frac{\partial \tau_{ij}}{\partial x_j}, \tag{2}$$

$$\frac{\partial (\rho e)}{\partial t} + \frac{\partial (\rho e u_j)}{\partial x_j} = -\frac{\partial (p u_i)}{\partial x_i} - \rho u_i g_i + \frac{\partial (\tau_{ij} u_i)}{\partial x_j} - \frac{\partial q_j}{\partial x_j} + \frac{\partial c_{pl} T s_{jl}}{\partial x_j}, \tag{3}$$

$$\frac{\partial (\rho Y_l)}{\partial t} + \frac{\partial (\rho Y_l u_j)}{\partial x_j} = \frac{\partial s_{jl}}{\partial x_j}, \tag{4}$$

where ρ is density, p is pressure, T is temperature, u_i is the velocity in the x_i direction, Y_1 is the mass fraction for the bottom fluid, Y_2 is the mass fraction for the top fluid, R is the gas constant, and the ideal gas law $p = \rho R T$ is enforced. Repeated indices imply summation. The specific total energy is

$$e = \frac{1}{2} u_i u_i + c_p T - \frac{p}{\rho}, \tag{5}$$

the viscous stress is assumed to be Newtonian and is

$$\tau_{ij} = \mu \left(\frac{\partial u_i}{\partial x_j} + \frac{\partial u_j}{\partial x_i} - \frac{2}{3} \frac{\partial u_k}{\partial x_k} \delta_{ij} \right), \tag{6}$$

the heat flux is written as

$$q_j = -k \frac{\partial T}{\partial x_j}, \tag{7}$$

and the species mass flux is defined as

$$s_{jl} = \rho D \frac{\partial Y_l}{\partial x_j}. \tag{8}$$

The initialization is discussed next. The upper fluid occupies the space where x_1 is greater than 0, and the lower fluid occupies the space where it is less than zero. This puts the interface at $x_1 = 0$ where the species mass fraction is smoothed using the error function since it is the exact solution to the diffusion equation between the species. For RTI to be present, it is required that the density be greater in the upper fluid than in the lower fluid. The normalized difference between the two densities is typically measured by a non-dimensional parameter called the Atwood number. For the compressible case, the density is not uniform in the two fluids. To avoid additional complications due to thermodynamic effects, we uniquely define the Atwood number as

$$A = \frac{W_2 - W_1}{W_2 + W_1}. \tag{9}$$

where W_l denotes the molecular weight of the fluid l, with $W_1 < W_2$.

For this study, the majority of fluid properties were taken to be the same between the two species. This includes the dynamic viscosity, μ, the heat conduction coefficient, k, the mass diffusion coefficient, D, and the gravitational acceleration, g_i, which is taken to only act in the vertical, x_1, direction. Finally, the gas constants are found based on the molecular weights as

$$R = \mathcal{R} \frac{Y_l}{W_l}, \tag{10}$$

where $\mathcal{R}$ is the universal gas constant. Following from this, the mixture specific heat at constant pressure, c_p, is calculated as a mass weighted average as well (i.e., $c_p = c_{pl} Y_l$).

Compressibility can be characterized by several parameters.[8,9] Here, we are mainly concerned with flow compressibility. In this case, the corresponding incompressible limit can be obtained by increasing the speed of sound through increasing the background pressure (or temperature), such that the densities are not affected. The Mach number associated with this compressibility is defined as the ratio of the gravity wave speed, $\sqrt{g\lambda}$, and the isothermal speed of sound, $a_0 = \sqrt{P_I/\rho_I}$, at the interface. This gives the definition of M as

$$M = \sqrt{\frac{\rho_I g \lambda}{P_I}}, \tag{11}$$

where the subscript I implies "interfacial". The interface density, ρ_I, is found using

$$\rho_I = \frac{P_I}{\mathcal{R}T_I}\left(\frac{W_1 + W_2}{2}\right). \tag{12}$$

Since the background state needs to be in hydrostatic equilibrium away from the interface, the Mach number defined above also characterizes the background stratification. The simulations presented here have the same ρ_I, W_l (which fixes the Atwood number), perturbation wavelength λ, and g, so that varying M results in a change of P_I and, subsequently, T_I.

For this study, three different sets of stratifications were used to initialize the simulations, namely isothermal, isentropic, and isopycnic. For the isothermal stratification, the density and pressure fields are

$$P(x_1) = P_I \exp\left(-\frac{g x_1}{R_l T_I}\right), \tag{13}$$

$$\rho(x_1) = \frac{P_I}{R_l T_I}\exp\left(-\frac{g x_1}{R_l T_I}\right), \tag{14}$$

where, in this case, T_I is not only the temperature for the interface, but is constant in the whole domain. For the isentropic case, the background stratification results from

$$P(x_1) = P_I\left(1 - \frac{\gamma}{\gamma - 1}\frac{g x_1}{R_l T_I}\right)^{\left(\frac{1}{\gamma-1}\right)}, \tag{15}$$

$$\rho(x_1) = \rho_l\left(1 - \frac{\gamma}{\gamma - 1}\frac{\rho_l g x_1}{P_I}\right)^{\left(\frac{1}{\gamma-1}\right)}, \tag{16}$$

and the temperature field is set to satisfy the equation of state. Finally, for the isopycnic case, ρ is set to be constant above and below the interface and the pressure field is set as

$$P(x_1) = -\rho_l g x_1 + P_I, \tag{17}$$

where P_I is added to ensure the correct interface pressure and T is again set to satisfy the equation of state. An example of the different stratifications can be seen in Figure 1.

Finally, to begin the RTI simulations, a small amplitude velocity perturbation is applied directly at the interface and the simulation is carried out from that state.[16] For the analogous vortex simulations, the same initial conditions are used with the discontinuity removed (i.e., $A = 0$) and an imposed velocity field.

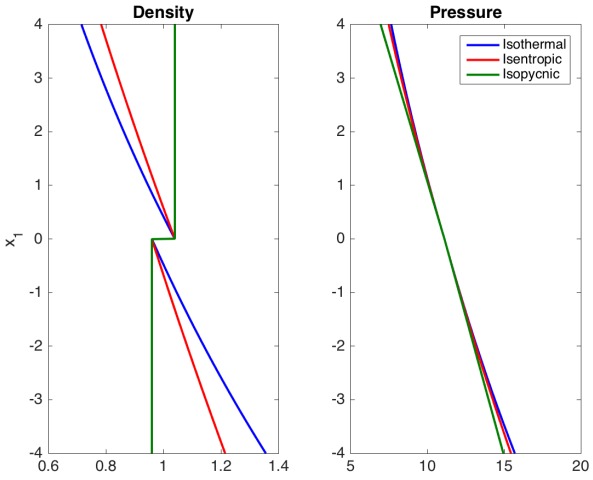

Figure 1. Density and pressure stratifications for $M = 0.3$ and $A = 0.04$ for the three different stratification types.

III. Numerical Method

The compact spatial localization of RTI development, at least during the early stages of growth, naturally lends itself to using state-of-the-art adaptive grid methods. The nature of the instability means that it will require a very long domain so that the late time growth can be fully captured, but also a very small grid spacing is required so that sharp gradients along the interfaces are well resolved. However, within the majority of the simulation domain, there is no flow development occurring far away from the interface. As a result, high grid resolution is initially only needed in the center of the domain. In order to minimize computational cost, a highly adaptive method is utilized so that high grid resolution is localized to only the areas in which there are important

flow features present. It has already been successfully shown that wavelet-based methods work very well to accomplish exactly this task.[15,16]

The Parallel Adaptive Wavelet Collocation Method (PAWCM) adapts on physical features to take advantage of this localization. PAWCM utilizes the inherent properties of wavelets to adapt the grid to physical quantities in areas of high variation. This leads to PAWCM automatically being able to add more resolution to areas in which important flow physics occur. PAWCM is already parallelized, has adaptive mesh refinement, direct error control, arbitrary dynamic domain decompositions for load balancing, and a tree-like data structure for efficient message passing. Any of the extra computational cost added by the wavelet transformation is inherently made up for by the large amounts of compression in the grid for a localized system such as the RTI problem examined here.[19–21] Using PAWCM for the RTI problem allows the simulation to run using only about 1-10% of the effective grid resolution.

PAWCM essentially works by taking the wavelet transform of the flow field variable of interest. The resulting wavelet basis functions are localized in both wave number and physical space. From there, the adaptation and compression of the field happens through thresholding. Essentially, a threshold parameter, ϵ, is defined and coefficients greater than that parameter are kept while coefficients less than are ignored. This results in the decomposition

$$u_{\geq}(x) = \sum_{k} c_k^0 \phi_k^0(x) + \sum_{j=0}^{\infty} \sum_{\mu=1}^{2^n-1} \sum_{\substack{l \\ |d_l^{\mu,j}| \geq \epsilon ||u||}} d_l^{\mu,j} \psi_l^{\mu,j}(x), \tag{18}$$

where u is a variable of interest, ϕ are the scaling functions on the coarsest level, ψ are the scaling interpolating functions on any arbitrary level, l and k represent physical grid points, and μ and j represent the wavelet family and level of resolution, respectively.[19,21]

As mentioned above, the wavelet thresholding technique results in any d below the threshold ϵ being effectively set to 0 and removed along with the wavelet it is associated with, resulting in the removal of the grid point. It is in the regions of high variability that d is also high, and so in smooth regions, d is low with respect to the j level of resolution and is most likely deemed insignificant. In the end, this results in a reduced-size grid with only these significant points, while still maintaining an error that is of the order of ϵ. In addition to these significant points, in order to ensure accuracy in time stepping, the points adjacent to any significant point on the the same j level are also retained. Finally, finite differences are used to approximate derivatives with the addition of ghost points to ensure that the order of accuracy of the simulation is maintained. To do this finite differencing, second generation wavelets are used so that many different orders of accuracy are easily accessible.[19,21]

For boundary conditions, all of the faces besides the top and the bottom are taken as periodic. This allows for the symmetry of the simulation to be maintained while only needing to simulate a single wavelength. For the top and bottom of the domain, however, the boundary conditions are much more difficult. The hope is to maintain the illusion of a near-infinite domain, but due to the generation of pressure and shock waves from the application of the perturbation and the growth of the RTI, it must be ensured that there are little to no reflections of waves back into the domain, while also not affecting the background stratification. For this, the top and bottom boundary conditions have been set to shear-free slip boundaries with numerical diffusion buffer zones before them. This ensures that as a pressure wave is sent towards the top or bottom boundaries, the diffusion zone dissipates and dampens the wave causing there to be no need to fully resolve the wave as it hits the boundary. This approach also eliminates most of the wave energy before it can reflect. Any reflections that may be left over are weakened enough to have no consequence on the instability, and the domain is chosen to be large enough so that the instability does not reach these diffusion zones.[16]

IV. Results

A total of nine two-dimensional (2D) DNS simulations have been carried out for this investigation. These include the three stratification types (i.e., isothermal, isentropic, and isopycnic) along with three stratification strengths for each (i.e., $M = 0.3, 0.6,$ and 0.9). This selection of simulation parameters allows us to capture phenomena from the near-incompressible limit to high strength stratifications. Above $M = 1.0$, the isentropic case provides solutions that become imaginary before the domain is large enough to capture the entire flow, thus limiting the stratification strengths we are able to simulate. The domain size is taken

to be $[0,1]\times[-4,+4]$ with $A=0.04$. For the analogous vortex simulations, the domain size is taken to be $[-1,1]\times[-4,+4]$, and have been performed for the same stratifications as for the RTI case, for both bubbles propagating upwards and spikes downwards with the effective Atwood number taken to be zero. All of these simulations have been carried out at a Reynolds perturbation number of 5,000 for this study. This Reynolds number is defined as

$$Re_p = \sqrt{\frac{Ag\lambda^3}{(1+A)\nu^2}}, \tag{19}$$

and is a measure of the potential of the perturbation growth to the viscous forces. It also sets the minimum vortex scales achievable on the mesh.[17] Here, Re_p is kept constant between the RTI and vortex pair simulations.

A. Rayleigh-Taylor Instability simulations

All of the RTI simulations have been studied to understand how different stratifications affect the growth rate of the instability. As mentioned before, the effects of these various compressible stratifications are not fully understood. Figure 2 on page 8 shows a comparison of the growth corresponding to all of the stratifications at the same time for all of the different Mach numbers. It is quite clear that increasing the strength of the background stratification for the isothermal case has a large effect on the growth of the instability. As the Mach number increases, the growth is suppressed more and more, causing the instability to reach a quasi-steady, diffusion-dominated mixing state. The higher the strength, the quicker this state is reached. When the stratification is strong enough, vortical structures that would normally cause the instability to continue growing[16,17] are actually broken apart shortly after they form. Figure 3 on page 9 further shows the distance travelled by the tips of the bubble and spike, revealing that the stronger the stratification, the shorter the heights of the bubble and spike. For all the cases besides the near incompressible limit, the distances travelled seem to asymptote to some finite values. The difference between the asymptotic bubble and spike limiting height values is the maximum width that the stratification will allow the instability to grow before being completely suppressed.

The other stratifications, however, reveal very different trends, as shown in Figures 2 on page 8 and 3 on page 9 for the isentropic and isopycnic cases, respectively. These figures show that stratification effects are much less drastic in the isentropic and isopycnic cases as compared to the isothermal case. Firstly, the isentropic case shows a very similar trend to the isothermal case during the initial stages. As the Mach number increases, the stronger stratifications cause an initial suppression that increases with the Mach number. By approximately 4 units of time into the simulation, the differences start presenting themselves. In the isothermal case, the background stratification continues to suppress the generation of vorticity and at higher Mach numbers continues growing at decreased rates. For the isentropic case, however, higher stratifications are able to overcome their suppressive nature and generate enough vorticity to increase their growth rates. This leads to an increased growth rate at later times, and the higher Mach number stratifications are able to catch up to the the nearly incompressible case. Also in the isentropic case, these effects have a much greater impact on the growth of the spike, as compared to their impact on the growth of the bubble. This leads to large asymmetries developing between the bubble and spike shapes. The narrower spike shape, in turn, leads to a greater induced velocity on the tip since the vortical structures are closer to each other. As a result, the spike ends up accelerating at an even greater pace.

The isopycnic case initially looks very similar to the isentropic case. Initially, the suppression causes a delayed growth rate increasing with Mach number. At a similar time, the isopycnic case is able to overcome the higher Mach numbers and begins accelerating to catch up with the nearly incompressible limit. Shortly after that, however, the acceleration of the higher Mach number stratifications is actually able to completely overcome the growth rate of the incompressible limit. This leads to an increasing growth rate with Mach number, which is contrary to what we have seen in every other scenario. Also in contrast to the isentropic case, the isopycnic case has a much smaller asymmetry at the later times with respect to the growth of the bubble versus the spike. The exact reason as to the increased acceleration with the Mach number is still unknown, but is most likely due to the increasing temperature gradient in the background state.[22] In order to determine this more rigorously, however, additional research must be performed.

An alternative view of the RTI development can be seen in Figure 4 on page 10. This figure shows the growth rate of the spike over time and is shown with the various stratifications at the same Mach number presented together. The valuable takeaway from this view is that, with increasing Mach number,

the effects of background stratification cause an increasing difference in the plots. At a low Mach number, the effects of the background stratification are at a minimum, which is to be expected because it is a nearly incompressible state. Even for this weak stratification, the isopycnic case still has an increased growth rate while the isothermal case is the most suppressed. As the Mach number is increased, this disparity becomes larger and larger with the isopycnic case growing faster and faster, while the isothermal case is more and more suppressed.

B. Vortex Analogs

In order to better understand the mechanism of the growth and changes of the RTI, we can examine the vorticity field and terms in the vorticity equation, namely the compression, baroclinic torque, and viscous terms. When we investigate the vortical fields from the initial stages, it becomes apparent that the flow arises from the initial generation of a vortex pair. An image comparing the vorticity field generated by RTI and the vorticity field of a vortex pair can be seen in Figure 5 on page 11. This makes it apparent that the flow fields have important similarities. For meaningful comparisons, the total vorticity in the RTI flow is calculated when the first vortex pair is generated and is used as a parameter to set the strength and intensity of the vortex pair. From investigating the resulting flow of the matched vortex pair, we are able to gain deeper insights into the flow of the RTI.

In Figure 6 on page 12, the result for a relatively late-time vortex pair simulation for the isothermal case at Mach 0.3 is shown. The figure shows the vorticity field along with the compression term and baroclinic torque generation term from the vorticity equation. There are two separate simulations, one to investigate the pair propagating upwards as the bubble in the RTI case, and one propagating downwards to mimic the spike in the RTI case. In the isothermal case, even at the low Mach number of 0.3, the suppression of the vortex pair by the background stratification is readily apparent. This figure shows that, even though the vortex pair is strong enough to begin moving through the domain, the movement of fluid causes the generation of a similar, but opposite, vorticity field around the vortex pair. This happens through the baroclinic torque production term, and results in the suppression of the vortex pair movement and the eventual destruction of the pair as a whole. It is evident that this happens in both the bubble and the spike scenarios, and the full suppression also happens faster as the Mach number is increased.

In order to better understand the interaction of the background stratification with the RTI, the vortex pair simulations are extended to also investigate the effects of the isopycnic and isentropic stratifications on the vortex pairs. For the isopycnic case, as expected, the effects are minimal with the vortex pair continuously moving through the domain until the end wall is reached. This shows that the stratification has little effect on the pair, which correlates with the fact that the isopycnic stratification has the fastest growth of the RTI cases. The isentropic case, however, lends itself to a more interesting result. Figure 7 on page 13 shows a comparison of the results of the vortex pair simulations for the isothermal and isentropic stratifications at the same time. The results are plotted for Mach numbers of 0.3 and 0.9, and the corresponding density is shown in the center of the domain.

From these images, differences in the flow become apparent. In both Mach number cases, the isothermal case is greatly suppressed in comparison to the isentropic case. As discussed before, this effect arises from the baroclinic torque production term in the vorticity equation. The flow field alters the density field in such a way that the baroclinic torque term has to adjust to correct the relationship of the density and pressure. Consequently, the density field is changed at the location of the vortex pair. At the Mach number of 0.9, the suppression is great enough that at this time, the vortex pair is completely destroyed and the resulting vorticity field is essentially random noise leading to a mixing regime. In the isentropic case, however, the baroclinic torque term is never disturbed in a way to lead to the surrounding opposite vorticity field that appears in the isothermal case, which shows itself in the density field remaining smooth. This allows the vortex pair to quickly propagate through the fluid unhindered. As the Mach number increases, we do see an increased dissipation of vorticity resulting in the propagation to be slowed, but the vortex pair is able to move, unlike in the isothermal case. Finally, the increased background stratification of the isentropic case results in the vortex pair being pushed closer together. This is another trait that appears in the RTI case as well. In the vortex pair case, the stratification causes the dissipation of the vorticity field, but in the RTI case, the potential energy of the instability allows it to keep moving, albeit at a much reduced rate, after the vorticity is suppressed. By also moving the pair closer together, there should be an increased induced velocity of the spike tip. This has been shown to be true for RTI, and thus these simulations relate well.

Based on this vorticity analysis, we can predict whether an instability will be fully suppressed or allowed

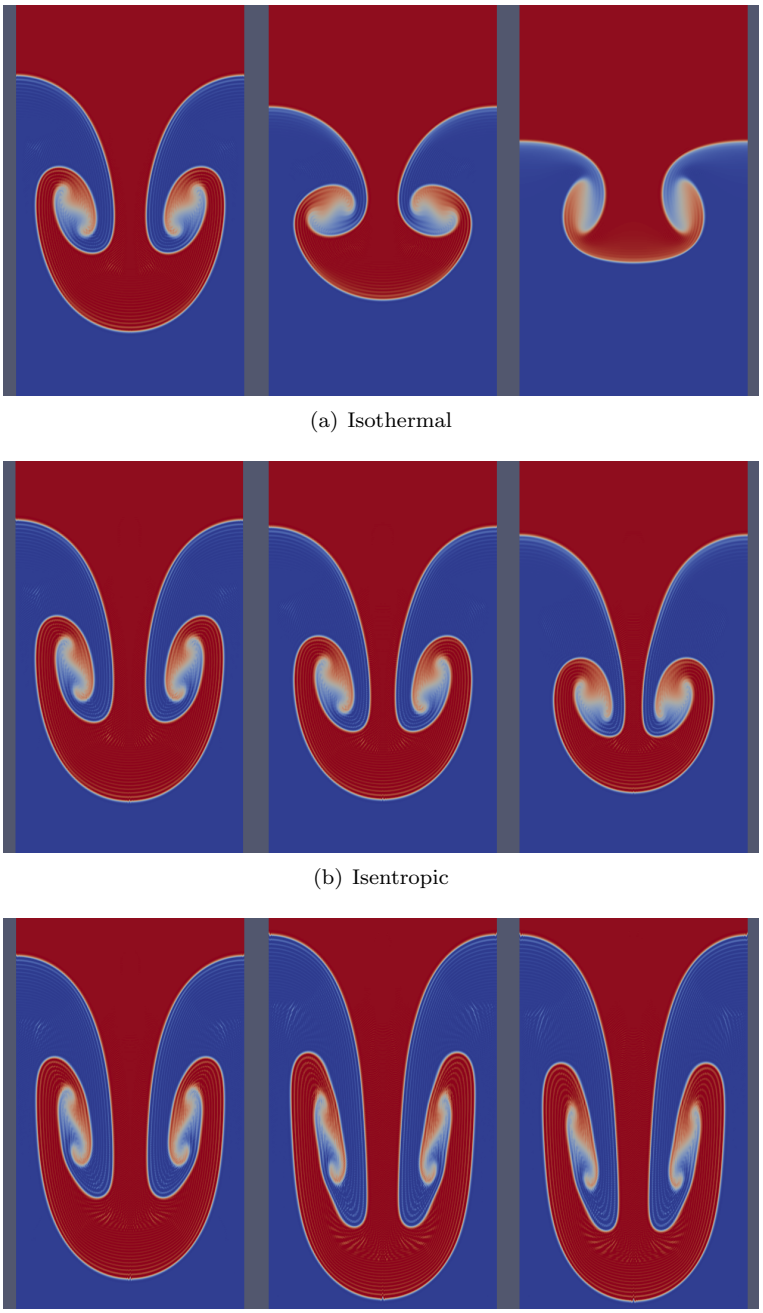

(a) Isothermal

(b) Isentropic

(c) Isopycnic

Figure 2. A comparison of the mass fraction contours for all the stratifications considered. The isothermal case is at the top, followed by the isentropic, and then the isopycnic. Going from left to right, the Mach number is increasing in each simulation. The leftmost is Mach of 0.3, the center 0.6, and the right 0.9. All of the simulations are shown at the same time. The heavy fluid is shown in red, and the light fluid is shown in blue.

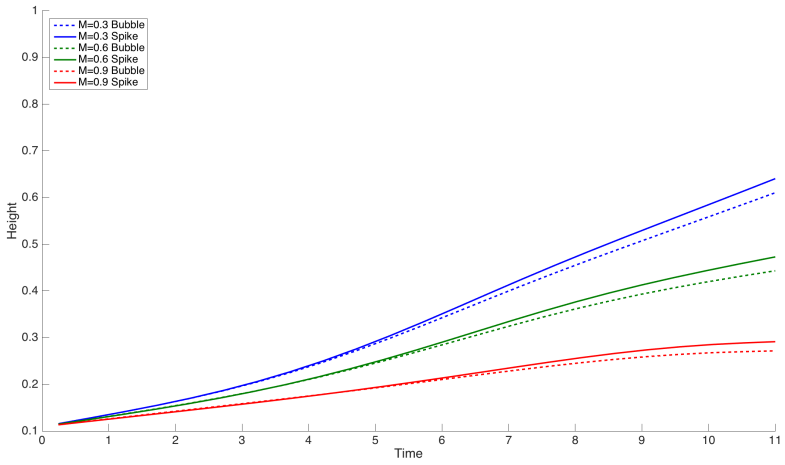

(a) Isothermal

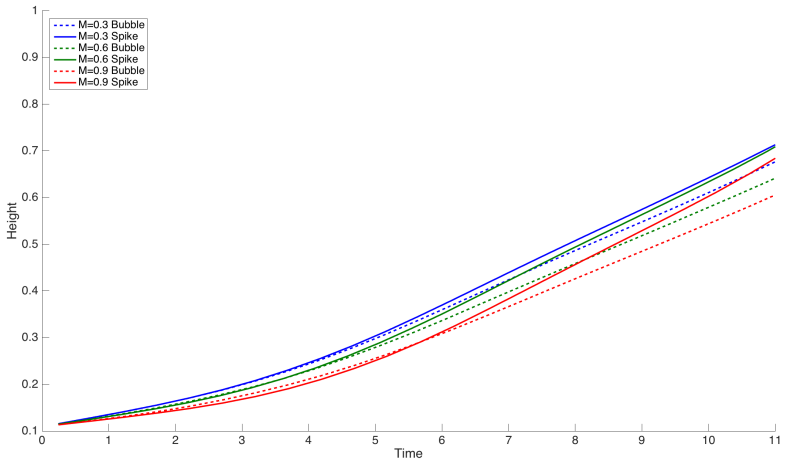

(b) Isentropic

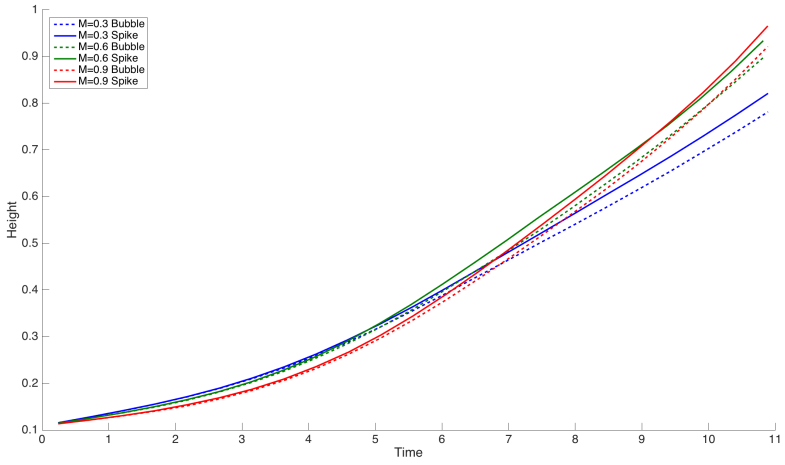

(c) Isopycnic

Figure 3. A comparison of the heights of the spike and bubble tips for the instability growth over time. The top plot shows the isothermal case, the middle shows the isentropic, and the bottom shows the isopycnic. In each plot blue represents a Mach number of 0.3, green is 0.6, and red is 0.9. Solid lines show the height of the spike dropping downwards while dashed lines show the height of the bubble rising.

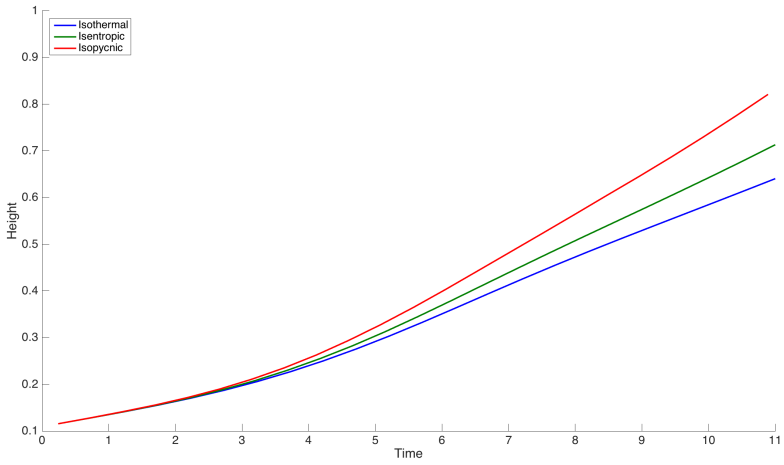

(a) M=0.3

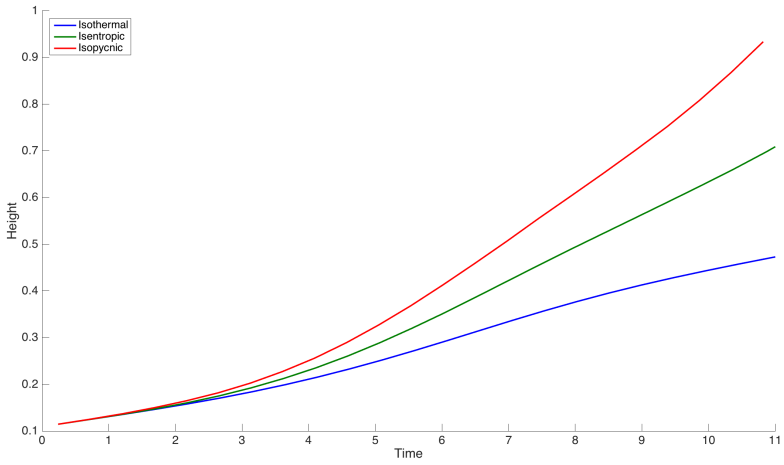

(b) M=0.6

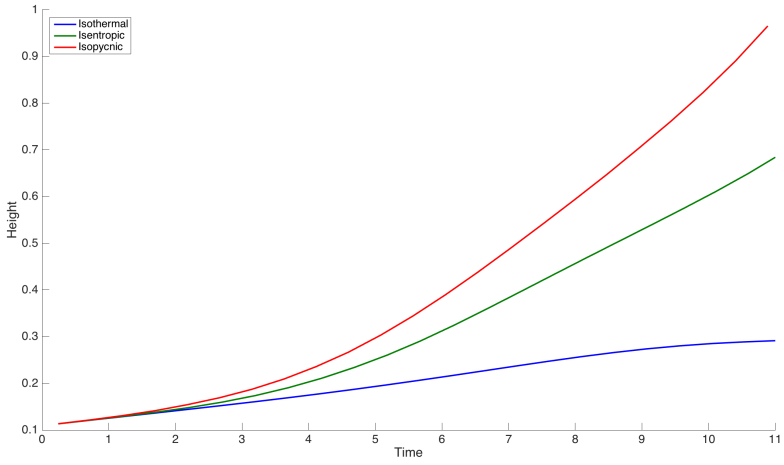

(c) M=0.9

Figure 4. An alternative view of the growth rates of the instability in the various stratifications. The top figure displays all the background stratifications at a Mach number of 0.3, the middle at 0.6, and the bottom at 0.9. The blue lines show the isothermal case, green is the isentropic case, and red is the isopycnic case. Each plot displays the growth rate of just the spike over time.

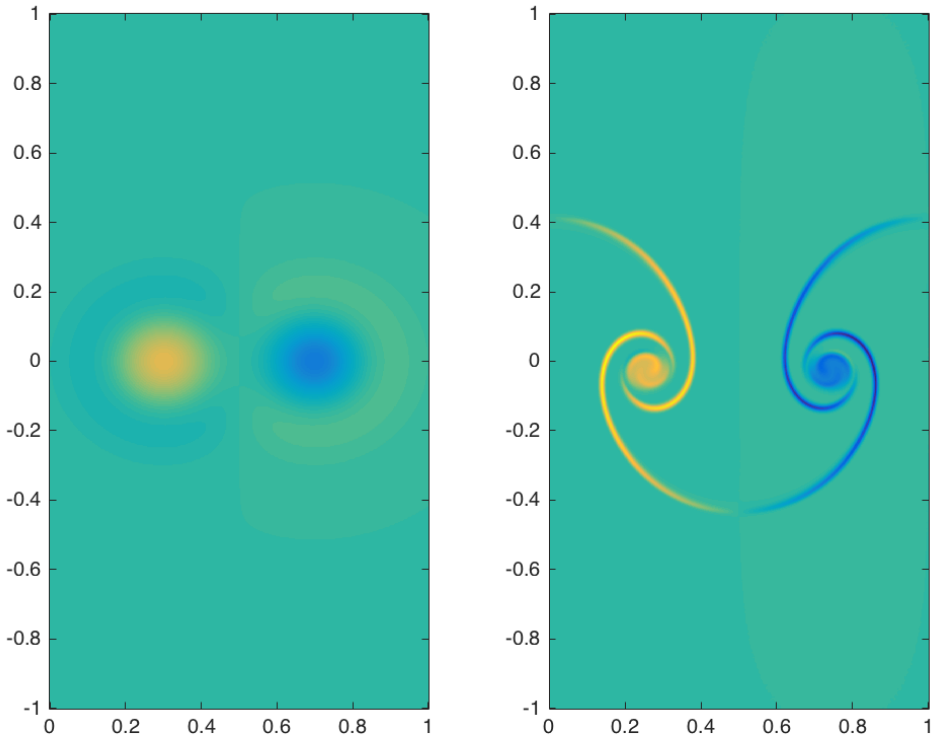

Figure 5. A comparison of the vorticity field generated by a vortex pair (left), and Rayleigh-Taylor instability (left).

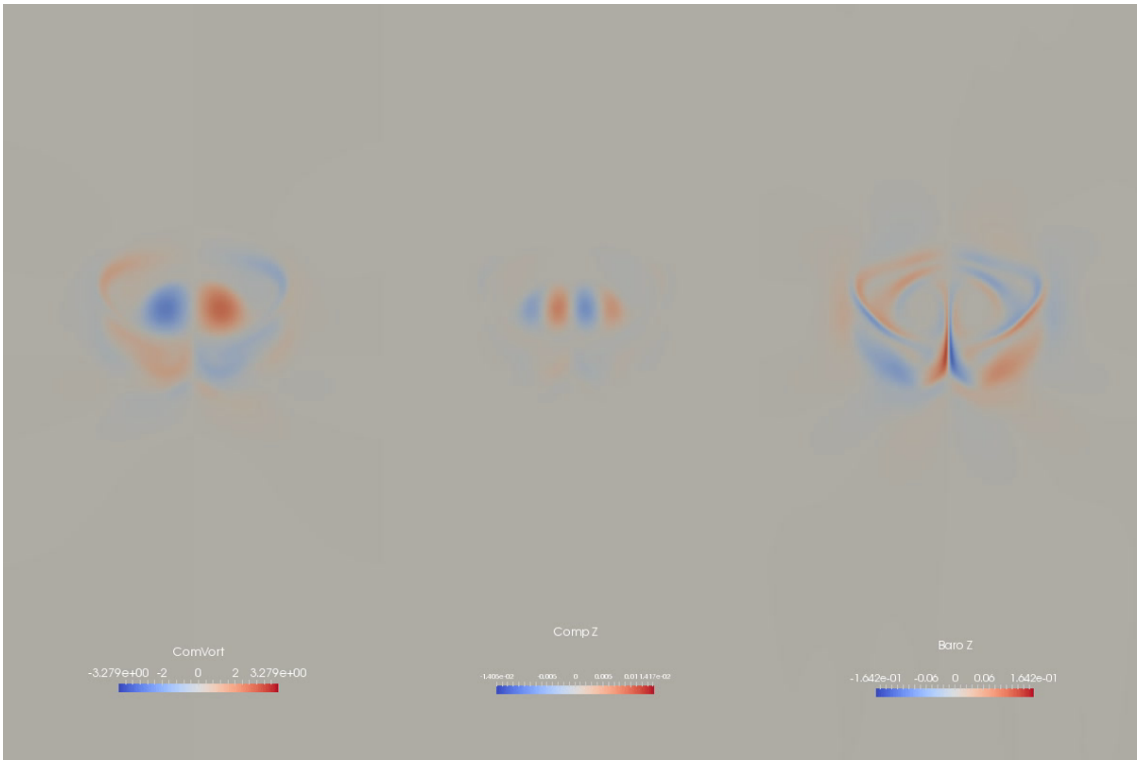

(a) Bubble

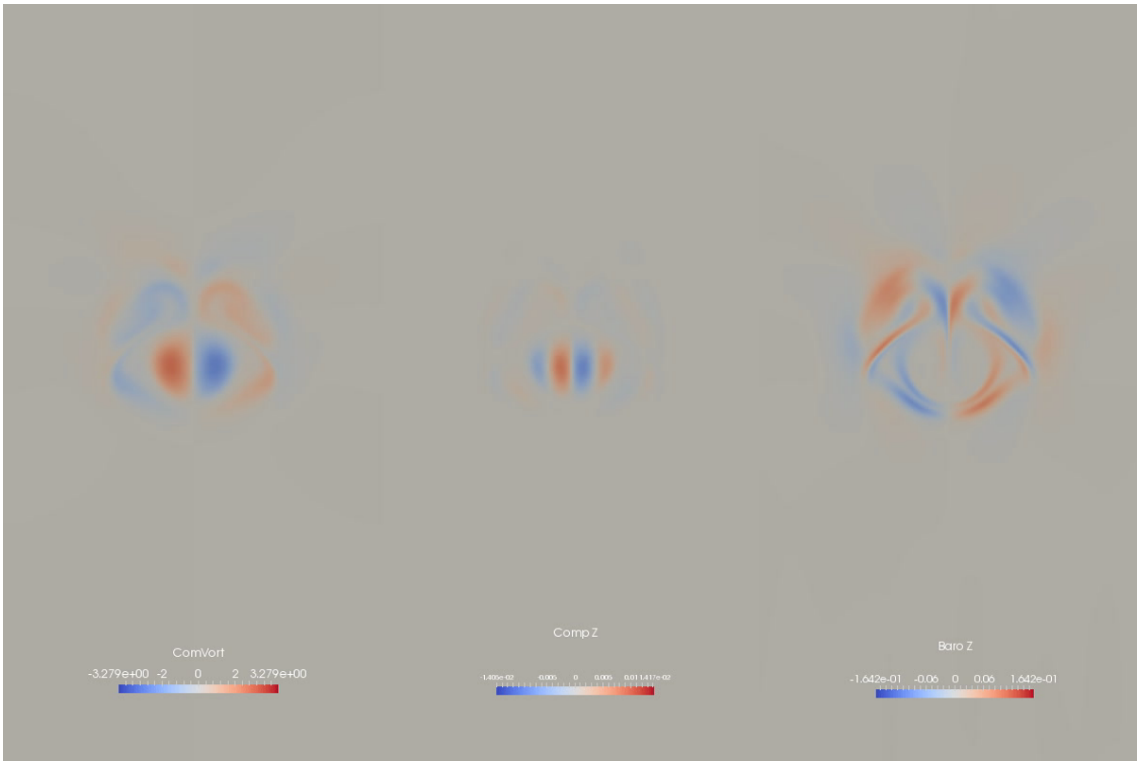

(b) Spike

Figure 6. A comparison of the vortical structures and their development for a vortex pair propagating up (top) like a bubble and down (bottom) like a spike in the isothermal stratification of $M = 0.3$. The left plot shows the vorticity, center the compression, and the right plot shows the baroclinic torque term.

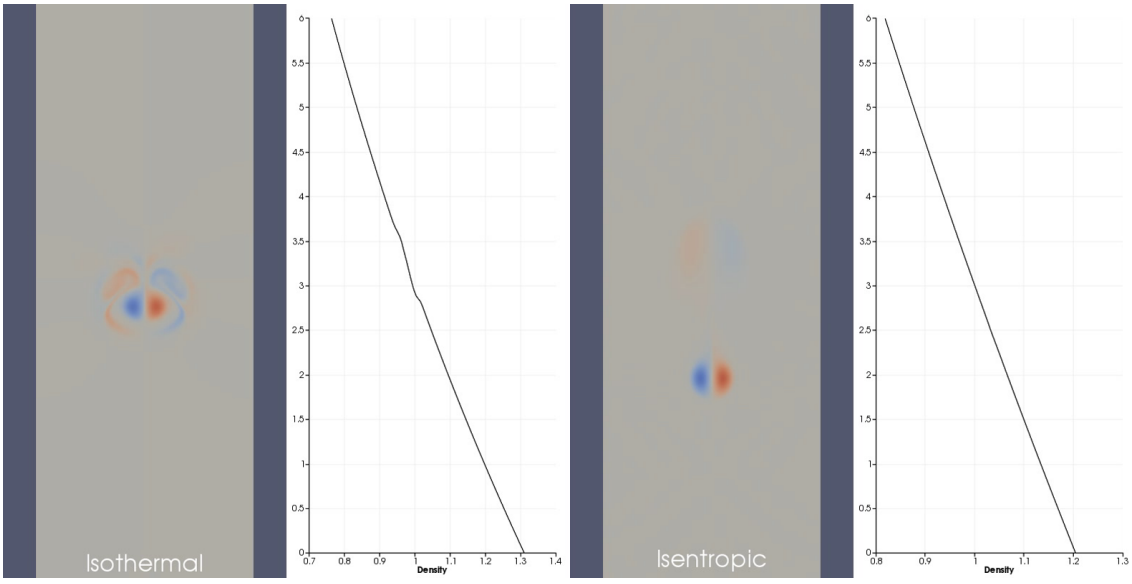

(a) M=0.3

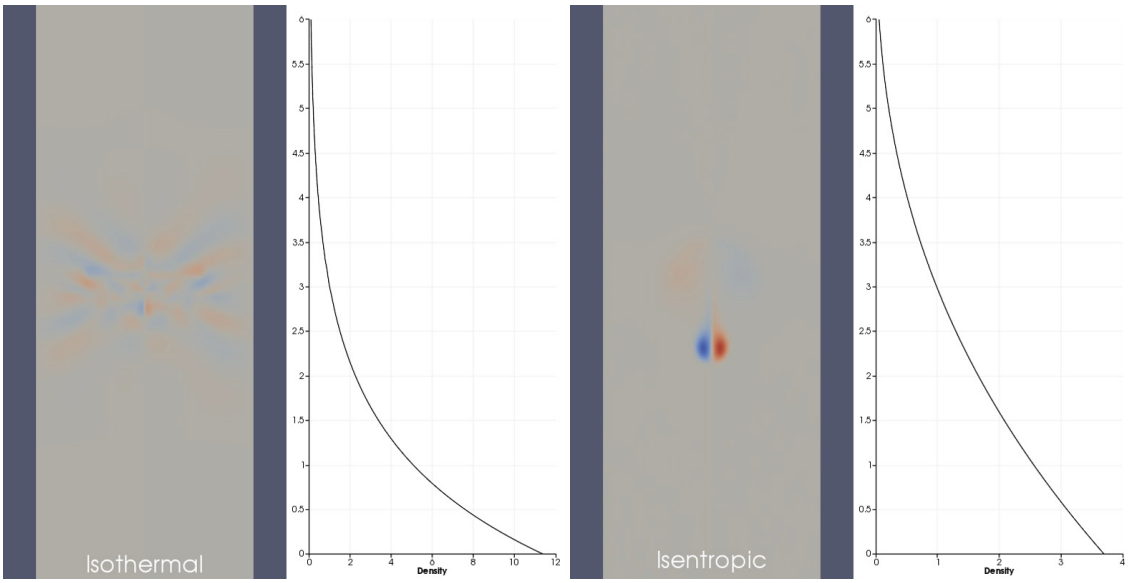

(b) M=0.9

Figure 7. A comparison of the vortex pair propagation through stratified media. On the left of each image are the results for the isothermal stratification, and the right shows the isentropic stratification results. The main representation is the vorticity field, and to the right of each vortical field is the resulting density along the centerline of the domain. The top image is for a Mach number of 0.3, and the bottom image for 0.9. Time is the same for all images.

to continue propagating based on the vortex pair interaction with background stratification. Based on this knowledge, the vortex pair simulations only predict the complete destruction of the vortical field in the isothermal scenario, which corroborates our RTI results. From this logic, it can be predicted that given a longer running time, the isentropic and isopycnic cases should continue growing and evolving and never be fully suppressed.

V. Conclusions

Simulations of the Rayleigh Taylor instability have been carried out for isothermal, isentropic, and isopycnic background stratifications. Each stratification was tested at various strengths corresponding to isothermal Mach numbers of 0.3, 0.6, and 0.9. It was observed that the isothermal stratification leads to the full suppression of the instability for all but the weakest background stratification, but even the weakest background stratification is significantly suppressed in comparison to the growth with the other stratifications.

For the isentropic stratification, it was found that the initial growth is suppressed in a similar way with the isothermal stratification, but at late times there is an acceleration of the bubble and spike tips, and the high Mach number growth approaches that of the lowest Mach number. Also, the isentropic stratification affects the spike more than the bubble, exaggerating the asymmetry between the two.

Finally, the isopycnic stratification was found to also lead to the initial suppression in the early growth stages with increasing Mach number. As the instability is allowed to grow in the isopycnic scenario, however, both the bubble and spike accelerate at greater rates with higher Mach number stratifications. The ultimate mechanism of this scenario is still under investigation and will be revealed through further research efforts.

These conclusions were tested against vortex pair analogs. The tests showed that the baroclinic torque vorticity term caused the greatest effect in the isothermal scenario, resulting in greater suppression of the growth. The vortex pair studies also helped to shed some light on how the isentropic stratification results in the asymmetry of the bubble and spike and why the spike is able to accelerate as it does. Further research will involve exploring all of these same effects, but with higher resolution and higher Reynolds number cases.

VI. Acknowledgements

This work was made possible in part by funding from the LDRD program at Los Alamos National Laboratory through project number 20150568ER. SAW was supported by Los Alamos National Laboratory, under Grant No. 316898. Computational resources were provided by the LANL Institutional Computing (IC) Program.

References

[1]Rayleigh, L., "Investigation of the character of the equilibrium of an incompressible heavy fluid of variable density," *Proceedings of the London mathematical society*, Vol. 14, 1884, pp. 170–177.

[2]Taylor, G., "The Instability of Liquid Surfaces when Accelerated in a Direction Perpendicular to their Planes. I," *Proceedings of the Royal Society A: Mathematical, Physical and Engineering Sciences*, Vol. 201, No. 1065, Mar 1950, pp. 192–196.

[3]Betti, R., Goncharov, V. N., McCrory, R. L., and Verdon, C. P., "Growth rates of the ablative Rayleigh-Taylor instability in inertial confinement fusion," *Physics of Plasmas*, Vol. 5, No. 5, May 1998, pp. 1446.

[4]Jordan IV, G. C., Fisher, R. T., Townsley, D. M., Calder, A. C., Graziani, C., Asida, S., Lamb, D. Q., and Truran, J. W., "Three-Dimensional Simulations of the Deflagration Phase of the Gravitationally Confined Detonation Model of Type Ia Supernovae," *The Astrophysical Journal*, Vol. 681, No. 2, Jul 2008, pp. 1448–1457.

[5]Hachisu, I., Matsuda, T., Nomoto, K., and Shigeyama, T., "Rayleigh-Taylor instabilities and mixing in the helium star models for Type Ib/Ic supernovae," *Astrophysical Journal, Part 2 - Letters*, Vol. 368, 1991, pp. L27–L30.

[6]Cabot, W. H. and Cook, A. W., "Reynolds number effects on Rayleigh-Taylor instability with possible implications for type Ia supernovae," *Nature Physics*, Vol. 2, No. 8, 2006, pp. 562–568.

[7]Lewin, W. H. G., van. Paradijs, J., and van den Heuvel, E. P. J., *X-ray binaries*, Cambridge University Press, 1997.

[8]Livescu, D., "Numerical simulations of two-fluid turbulent mixing at large density ratios and applications to the Rayleigh-Taylor instability." *Philosophical transactions. Series A, Mathematical, physical, and engineering sciences*, Vol. 371, No. 2003, Nov 2013, pp. 20120185.

[9]Livescu, D., "Compressibility effects on the Rayleigh-Taylor instability growth between immiscible fluids," *Physics of Fluids*, Vol. 16, No. 1, 2004, pp. 118.

[10]Gauthier, S. and Le Creurer, B., "Compressibility effects in Rayleigh-Taylor instability-induced flows," *Philosophical Transactions of the Royal Society of London A: Mathematical, Physical and Engineering Sciences*, Vol. 368, No. 1916, 2010.

[11]Sharp, D., "An overview of Rayleigh-Taylor instability," *Physica D: Nonlinear Phenomena*, Vol. 12, No. 1, 1984, pp. 3–18.

[12]Boffetta, G. and Mazzino, A., "Incompressible Rayleigh-Taylor turbulence," *Annual Review of Fluid Mechanics*, Vol. 49, 2017, pp. 119–143.

[13]Dimonte, G., Youngs, D. L., Dimits, A., Weber, S., Marinak, M., Wunsch, S., Garasi, C., Robinson, A., Andrews, M. J., Ramaprabhu, P., Calder, A. C., Fryxell, B., Biello, J., Dursi, L., MacNeice, P., Olson, K., Ricker, P., Rosner, R., Timmes, F., Tufo, H., Young, Y.-N., and Zingale, M., "A comparative study of the turbulent Rayleigh-Taylor instability using high-resolution three-dimensional numerical simulations: The Alpha-Group collaboration," *Physics of Fluids*, Vol. 16, No. 5, Apr 2004, pp. 1668.

[14]Lafay, M.-A., Le Creurer, B., and Gauthier, S., "Compressibility effects on the Rayleigh-Taylor instability between miscible fluids," *Europhysics Letters (EPL)*, Vol. 79, No. 6, Sep 2007, pp. 64002.

[15]Reckinger, S. J., Livescu, D., and Vasilyev, O. V., "Adaptive wavelet collocation method simulations of RayleighTaylor instability," *Physica Scripta*, Vol. T142, No. T142, Dec 2010, pp. 014064.

[16]Reckinger, S. J., Livescu, D., and Vasilyev, O. V., "Comprehensive numerical methodology for direct numerical simulations of compressible Rayleigh-Taylor instability," *Journal of Computational Physics*, Vol. 313, 2016, pp. 181–208.

[17]Wei, T. and Livescu, D., "Late-time quadratic growth in single-mode Rayleigh-Taylor instability," *Physical Review E*, Vol. 86, No. 4, Oct 2012, pp. 046405.

[18]Williams, F. A. F. A., *Combustion theory : the fundamental theory of chemically reacting flow systems*, Addison/Wesley Pub. Co, 1985.

[19]Vasilyev, O. V. and Bowman, C., "Second-Generation Wavelet Collocation Method for the Solution of Partial Differential Equations," *Journal of Computational Physics*, Vol. 165, No. 2, 2000, pp. 660–693.

[20]Schneider, K. and Vasilyev, O. V., "Wavelet Methods in Computational Fluid Dynamics*," *Annual Review of Fluid Mechanics*, Vol. 42, No. 1, Jan 2010, pp. 473–503.

[21]Nejadmalayeri, A., Vezolainen, A., Brown-Dymkoski, E., and Vasilyev, O. V., "Parallel adaptive wavelet collocation method for PDEs," *Journal of Computational Physics*, Vol. 298, 2015, pp. 237–253.

[22]Gerashchenko, S. and Livescu, D., "Viscous effects on the Rayleigh-Taylor instability with background temperature gradient," *Physics of Plasmas*, Vol. 23, 2016, pp. 072121.